

Synthesis of [60]fullerene derivatives bearing five-membered heterocyclic wings and an investigation of their photophysical kinetic properties

Leandro J. Santos^a, Ana S.P. Gonçalves^b, Klaus Krambrock^b, Maurício V.B. Pinheiro^b, Marcos N. Eberlin^c, Boniek G. Vaz^c, Rossimiriam P. de Freitas^{d,*}, Rosemeire B. Alves^d

^a Universidade Federal de Viçosa, Campus de Florestal, Rodovia LMG, 818-km 6, CEP: 35690-000 s/n, Florestal, MG, Brazil

^b Departamento de Física, Instituto de Ciências Exatas, Universidade Federal de Minas Gerais, Avenida Antônio Carlos 6627, CEP: 31270-901, Belo Horizonte, MG, Brazil

^c Laboratório ThoMSon de Espectrometria de Massas, Instituto de Química, Universidade Estadual de Campinas, Campus Zeferino Vaz Bloco A6-111, CEP:13083-970 CP 6154, Barão Geraldo, Campinas, SP, Brazil

^d Departamento de Química, Instituto de Ciências Exatas, Universidade Federal de Minas Gerais, Avenida Antônio Carlos 6627, CEP: 31270-901, Belo Horizonte, MG, Brazil

ARTICLE INFO

Article history:

Received 26 January 2010

Received in revised form

14 September 2010

Accepted 11 October 2010

Available online 15 October 2010

Keywords:

Fullerene C₆₀ derivatives

Electron paramagnetic resonance

Reactive oxygen species

Photosensitizers

ABSTRACT

The preparation, characterization and photophysical properties of six new stable [6,6]-closed fullerene cycloadducts bearing five-membered heterocycles are described. The modified [60]fullerenes are obtained by a simple and rapid synthesis via a Bingel-type reaction with tetrazole and oxadiazole malonate derivatives. The photophysical kinetics of these new fullerene derivatives in toluene solution under ultraviolet illumination (375 nm, UVA) are studied by electron paramagnetic resonance and free-radical spin-trapping using α -phenyl-*N*-tert-butyl nitron as a spin-trap. The results are compared with pure [60]fullerene and [6,6]-phenyl C₆₁ butyric acid methyl ester (C₆₀-PCBM). It is concluded that for all six new compounds as well as pure [60]fullerene and PCBM both superoxide and singlet oxygen are produced in the first stages of UVA illumination following the type I and II mechanisms, respectively. In all cases singlet oxygen is produced as the primary dominant species; however, the type I mechanism always occurs in parallel with type II. In the end, the superoxide is self-dismuted into hydroxyl radicals, thus yielding PBN-OH^{*} spin adducts ($g = 2.007$ and $a_{\text{hf}}(^{14}\text{N}) = 1.54$ mT). The kinetic reaction constants and their efficiencies in the production of reactive oxygen species at 375 nm and per mW of absorbed power are determined. The experimental results are consistent with an autocatalytic reaction model in which the system evolves under UVA illumination, with superoxide catalyzing the conversion of singlet oxygen into more superoxide.

© 2010 Elsevier B.V. All rights reserved.

1. Introduction

Since the discovery of fullerenes in 1985 [1] and their subsequent availability in macroscopic quantities [2], the chemical and physical properties of functionalized fullerenes have attracted considerable attention. Fullerene derivatives have many applications, such as in non-linear optical devices [3,4], photosensitizers [5–8], photovoltaic cells [9], and biomedicine [10–13]. To design and construct new molecules with novel and attractive properties and applications, judicious structural modifications of [60]fullerene are required [14,15]. These modifications can be achieved either by non-covalent binding with other molecules (for example, C₆₀ and C₇₀ fullerenes with a derivatized Zn-phthalocyanine [16] for applications in hybrid photovoltaics or as photosensitizers for pho-

todynamic therapy in the visible spectral range) or by covalently modifying the fullerenes to obtain, for example, polyhydroxylated fullerenes with water-solubility and the free-radical scavenging properties required for applications in anti-oxidant drugs [17].

Nevertheless, the covalent modification of [60]fullerene with heterocyclic “wings” containing two or more nitrogen atoms has only recently been explored. For example, the hexakis adduct 1 (Fig. 1) [18] was prepared under copper-mediated Huisgen 1,3-dipolar cyclo-addition, and it displayed interesting electrochemical properties. In addition, the fullerene adduct 2, bearing a triazole group, was recently synthesized by Chen et al. [19]; it exhibited electron transport properties that may be useful in the construction of organo-electronic devices.

Recently, we have synthesized the first fullerene derivative linked with a tetrazole unit 3 (Fig. 1) and determined that it exhibits photophysical properties suitable for the production of reactive oxygen species (ROS) by ultraviolet A (UVA) photosensitization [20]. This derivative may have potential use as a photosensitizer in photodynamic therapy (PDT). In continuation of that work, the

* Corresponding author. Tel.: +55 3134095721; fax: +55 3134095700.

E-mail addresses: rossipdf@yahoo.com.br (R.P. de Freitas), brondi@netuno.lcc.ufmg.br (R.B. Alves).

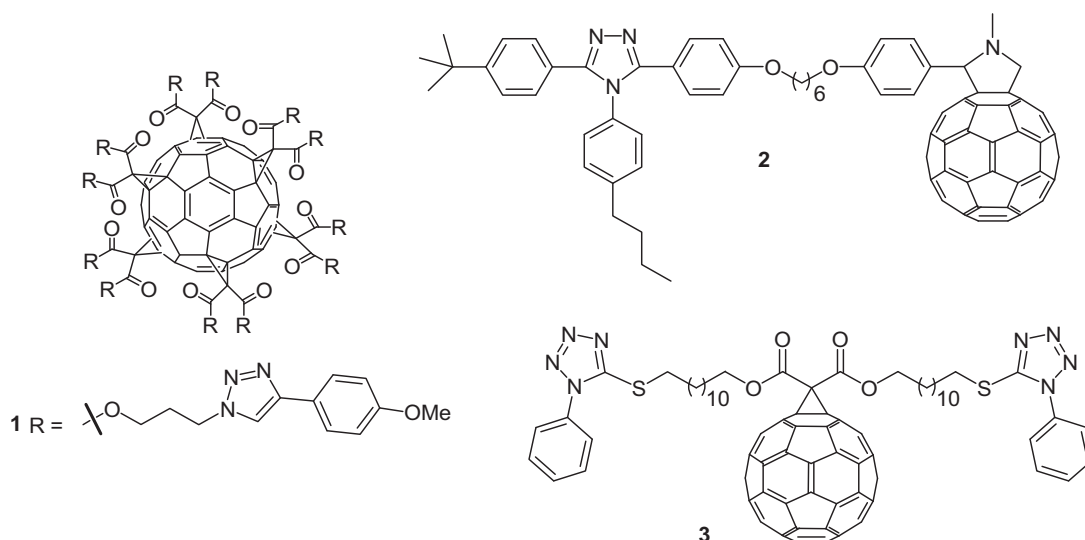


Fig. 1. [60]Fullerene derivatives containing heterocycles.

synthesis, characterization and photophysical properties of six new [60]fullerene derivatives containing either tetrazole or oxadiazole units are reported here.

2. Experimental

2.1. Materials and experimental setup

Reagents and solvents were purchased as reagent grade and used without further purification. Tetrahydrofuran (THF) was distilled over sodium benzophenone. Dry acetone was prepared after agitation with potassium carbonate for 24 h at room temperature and then distilled. The azoles were obtained from Sigma–Aldrich. The C₆₀ (99.5%) and C₆₀-PCBM ([6,6]-phenyl C₆₁ butyric acid methyl ester) were obtained from M.E.R. Corporation and from SES RESEARCH, respectively.

The melting points were determined on a Mettler FP80HT apparatus and are reported uncorrected. The nuclear magnetic resonance (NMR) spectra were recorded on Bruker Avance DRX-200 or DRX-400 spectrometers. Chemical shifts are reported in δ units downfield from tetra-methylsilane, and the coupling constant (J) values are given in Hz. All of the compounds investigated in this work were characterized with optical absorption measured with an HP/Agilent 8453 UV–vis spectrophotometer. Fourier-transform mass spectroscopy (FT-MS) was performed with a LTQ FT ULTRA (ThermoScientific-7T-Germany) instrument with the TriVersa NanoMate system (Advion, USA) operating in the chip-based infusion mode and in the positive ion mode using a silicon-based integrated nano-electrospray microchip. Column chromatography was performed with silica gel 60, 70–230 mesh (Merck). A commercial microwave oven (Panasonic Junior Smart NNS53BH) was specially modified [21] for organic synthesis and used to obtain the 12-bromododecane-1-ol.

All electron paramagnetic resonance (EPR) measurements were done at room temperature with a custom-built X-band spectrometer (9.38 GHz) using a commercial cylindrical cavity (Bruker) and a klystron (Varian). The magnetic field was produced by an electromagnet (Varian) and an automated current source (Heizinger). For detection, standard lock-in techniques (EG&G) and 100 kHz field modulation were employed (0.1 mT). Each spectrum had a scan time of 150 s. The microwave frequency was stabilized by an automatic frequency control up to five digits and the frequency was measured with a digital frequency meter (PTS). The magnetic field

calibration was done with a 2,2-diphenyl-1-picrylhydrazyl (DPPH) standard with $g = 2.0037$. The EPR measurements were performed as a function of illumination time, and with a microwave power of approximately 2 mW.

2.2. EPR spin-trapping methodology

The generation of ROS assisted by C₆₀ and its derivatives under UVA illumination was studied by EPR using the spin-trapping technique. Each sample consisted of two compounds in an air-saturated toluene solution: the spin trap PBN (α -phenyl-*N*-tert-butyl nitron) and one of the synthesized fullerene derivatives with concentrations of 300 mM and 1 mM, respectively. Two reference solutions, containing either pure C₆₀ or C₆₀-PCBM, were prepared with the same concentrations to compare their efficiency in ROS production. The samples were prepared under ambient laboratory light. A fixed volume of 100 μ L of the above solutions was added to a borosilicate EPR tube with a 3 mm inner diameter (Wilmad). An UVA solid state laser (Power Technology Inc.), with a wavelength of 375 nm and power of 16 mW, was used for illumination through the open top of the sample tube placed inside the EPR cavity. The spot had a diameter of 1.74 ± 0.15 mm, and the illuminated volume of the sample was 33.3 ± 2.9 μ L. All samples were measured under the same illumination conditions, with the exception of the spin quantification calibration measurements that are described in [supplementary data](#).

3. Experimental results and discussion

3.1. Synthesis and structural characterization of fullerene derivatives

The synthesis of key malonate derivatives containing a five-membered heterocyclic ring for the preparation of the new fullerene derivatives is achieved by two methods. The first method involves a [2+3] cycloaddition followed by reaction with commercial malonyl chloride, which produces the new tetrazole malonates. The second and simpler method is the alkylation of commercial tetrazoles and oxadiazole, which is followed by reaction with malonyl chloride to produce unknown azole malonates. Fig. 2 summarizes the synthesis of tetrazole malonates 10 and 11 and their use in the Bingel reaction to obtain fullerene derivatives. Initially, commercially available diol 4 is converted into its bromo deriva-

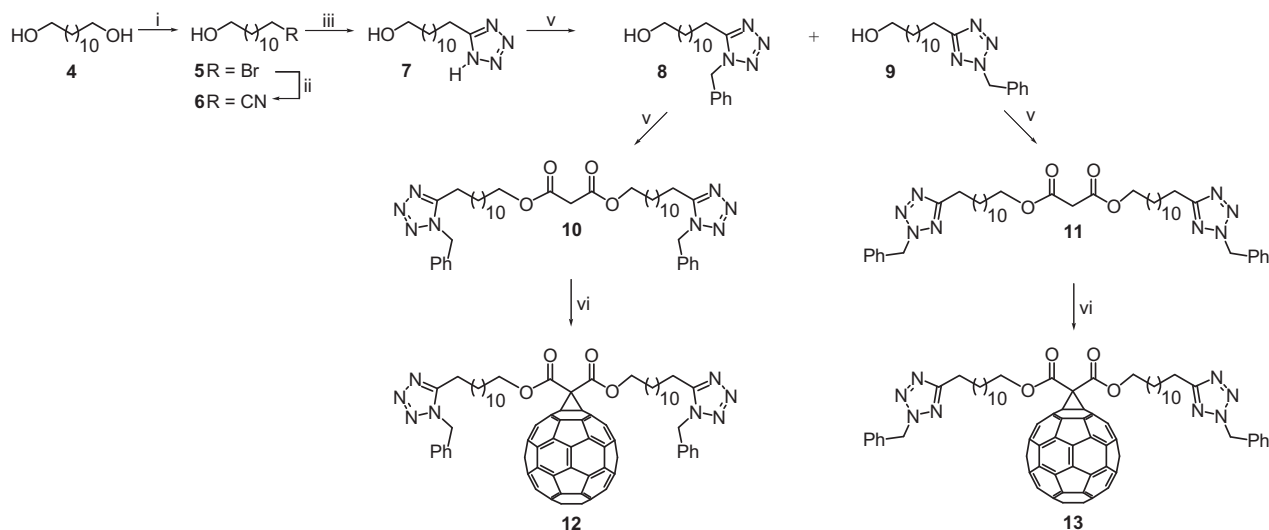


Fig. 2. Preparation of compounds **12** and **13**. Reagents and conditions: (i) HBr (48%), *n*-Bu₄NBr, MW, 4 min (51%); (ii) KCN, 18-crown-6 ether, CH₃CN, 80 °C, 48 h (76%); (iii) NaN₃, NH₄Cl, DMF, 140 °C, 20 h (100%); (iv) BnBr, K₂CO₃, acetone, 60 °C, 24 h, **8** (46%) and **9** (42%); (v) malonyl dichloride, pyridine, THF, room temperature, 5 h, **10** (50%) and **11** (51%) and (vi) C₆₀, I₂, DBU, toluene, room temperature, 5 h, **12** (31%, 65% based on recovered C₆₀) and **13** (40%, 70% based on recovered C₆₀).

tive **5** with a 51% yield [22]. Treatment of **5** with potassium cyanide and 18-crown-6 ether in CH₃CN [23] gives a 76% yield of nitrile **6**. The [2+3] cycloaddition of sodium azide and nitrile **6** with ammonium chloride in DMF [24] provides the 5-substituted tetrazole **7** in a quantitative yield. The structure of **7** is confirmed by ¹³C NMR, and the typical chemical shifts of C-tetrazolic are observed at 157.90 ppm [25]. Alkylation of **7** with benzyl bromide in dry acetone and anhydrous K₂CO₃ produces mixtures of *N*(1)- and *N*(2)-alkylation isomers [26]. After silica chromatography purification, two isomers, **8** and **9**, are isolated in 46% and 42% yield, respectively. These isomers are distinguished by the ¹³C chemical shifts of the *N*-alkyl group and verified with heteronuclear multiple bond correlation (HMBC) experiments. The HMBC contour plot shows the cross correlation between the tetrazole carbon and the CH₂ group linked to the vicinal nitrogen, due only to the ³*J* coupling constant for **8**. Isomers **8** and **9** are esterified separately with commercial

malonyl dichloride in pyridine and THF at room temperature, providing **10** and **11** in yields of 50% and 51%, respectively. Malonates **10** and **11** are subsequently transformed into their [60]fullerene mono-adducts **12** and **13**, respectively, following the conditions described by Nierengarten et al. [28].

Fig. 3 depicts the alkylation of the commercial tetrazoles **14**, **22**, **23** and oxadiazole **15** with 12-bromododecane-1-ol or commercial 6-chloroexan-1-ol. These reactions produce the alcohols **16**, **17**, **24(N-2)**, and **25(N-2)** in high yields, which are esterified with commercial malonyl dichloride to form the malonates **18**, **19**, **26(N-2)**, and **27(N-2)**, respectively. These malonates are subsequently transformed into their respective mono-adduct fullerene derivatives **20**, **21**, **28**, and **29** by the Bingel-type reaction [28], respectively, with yields between 36% and 42%. The structure and purity of all of the mono-adducts are confirmed by ¹H and ¹³C NMR spectroscopy (these results are listed in the supporting information).

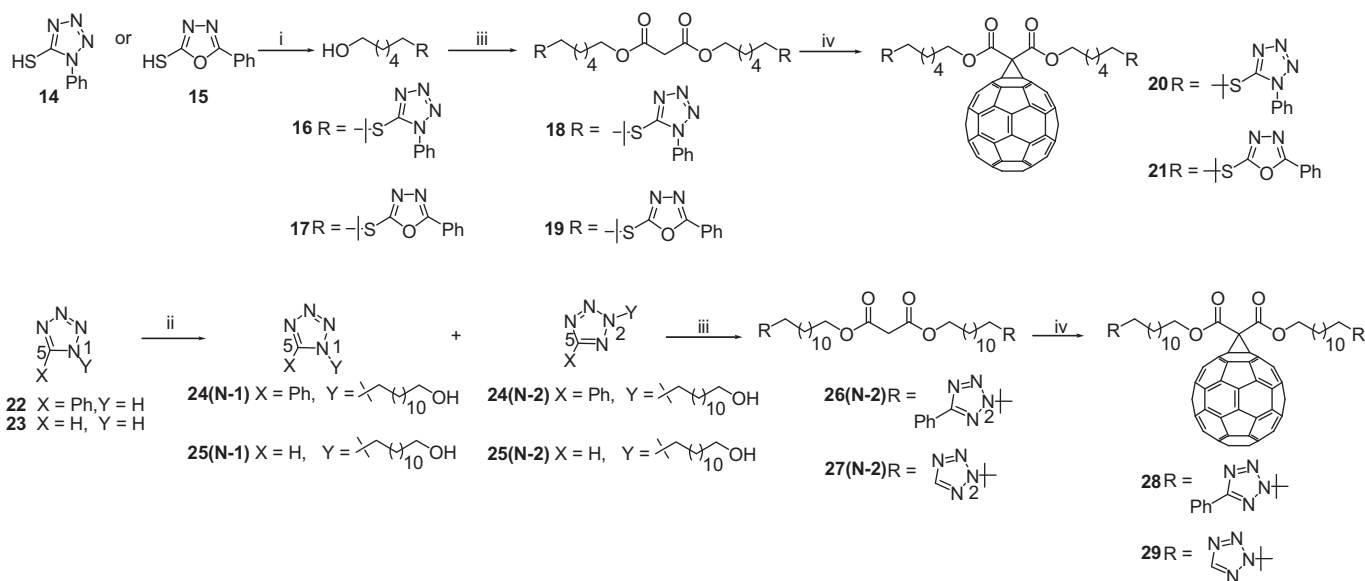


Fig. 3. Preparation of compounds **20**, **21**, **28** and **29**. Reagents and conditions: (i) 6-chloroexan-1-ol, K₂CO₃, acetone, 60 °C, 48 h, **16** (90%), **17** (60%); (ii) 12-bromododecane-1-ol, K₂CO₃, acetone, 60 °C, 24 h, **24(N-1)** (10%), **24(N-2)** (90%), **25(N-1)** (38%), **25(N-2)** (57%); (iii) malonyl dichloride, pyridine, THF, room temperature, 5 h, **18** (48%), **19** (60%), **26(N-2)** (55%), **27(N-2)** (35%) and (iv) C₆₀, I₂, DBU, toluene, room temperature, 5 h, **20** (36%, 77% based on recovered C₆₀), **21** (42%, 52% based on recovered C₆₀), **28** (39%, 43% based on recovered C₆₀), and **29** (38%, 50% based on recovered C₆₀).

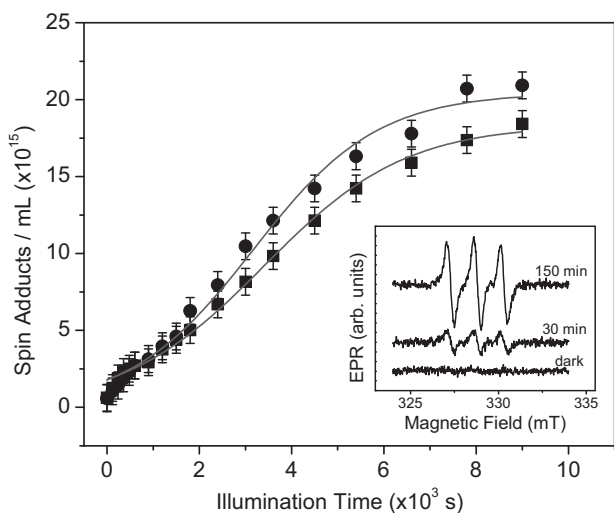


Fig. 4. Time evolution of the absolute PBN spin adduct concentration in an illuminated (UV laser: 375 nm, 16 mW, room temperature) toluene solution containing 1 mM C_{60} (■) or C_{60} -PCBM (●), and 300 mM of the spin trap PBN. The insert shows the EPR spectra for the C_{60} solution before illumination (dark) and after 30 and 150 min of illumination.

The ^{13}C NMR spectra of the mono-adducts show the characteristic signal [29] of the sp^3 -hybridized fullerene C atoms in the cyclopropane ring between 70 and 85 ppm, in addition to the signals between 136 and 150 ppm corresponding to the sp^2 -hybridized fullerene sphere. The methano bridge signal is observed in the region from 52 to 53 ppm.

The molecular compositions are also confirmed by ultra-high-resolution Fourier transform mass spectrometry with electrospray ionization. Molecular masses of all isotopologue ions within the $[M+H]^+$ clusters agree exceptionally well with calculated values and are within less than 1 ppm of those values. The MS/MS analysis of the protonated molecules via dissociations induced either by collisions or photons also shows structurally diagnostic dissociation patterns involving the heterocyclic wings, corroborating the assigned structures of the new fullerene derivatives.

For optical characterization, the fullerene solutions (0.02 mM in toluene) are placed in a standard quartz cuvette (10-mm thickness), and their spectra are recorded at room temperature. A pure air-saturated toluene sample is used for the baseline. All of the spectra are very similar. In the visible range (wavelength above 400 nm), the absorption is weak, but it increases drastically at shorter wavelengths (in the UVA and UVB ranges). The molar extinction coefficient (ϵ) is calculated for all samples at 375 nm, the wavelength of the laser diode used in the spin-trapping experiments. With the extinction coefficients ϵ , the amount of the laser power absorbed in the illuminated fraction of the sample volume of the EPR borosilicate sample tube (0.33 mL) is calculated by the Beer–Lambert law, taking into account the laser spot diameter (1.74 ± 0.15 mm) and the height of the solution in the tube (14.0 ± 0.5 mm) (these results are listed in supporting information).

3.2. EPR spin-trapping studies

Fig. 4 shows the absolute concentration of PBN spin adducts generated in a toluene solution of C_{60} or commercial C_{60} -PCBM as a function of illumination time. The EPR spectra are measured at room temperature. The C_{60} and C_{60} -PCBM concentrations are 1 mM, whereas the PBN concentration is 300 mM. The curves are calculated from a series of EPR spectra after different illumination times using the TEMPOL calibration data. The EPR spectra from C_{60} and all of the other investigated fullerene derivatives are dominated by

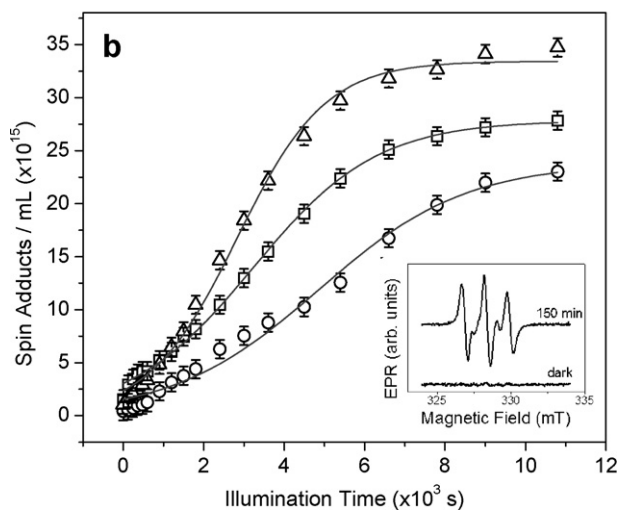
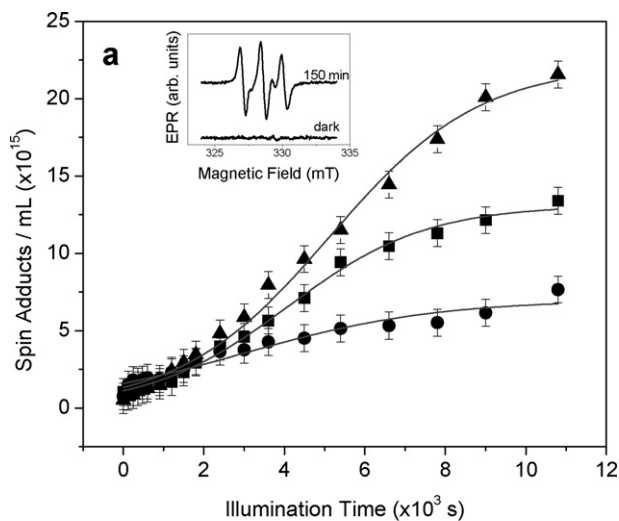


Fig. 5. Time evolution of the absolute PBN spin adduct concentration in the illuminated toluene solutions containing fullerene derivatives (at 1 mM) and the spin trap PBN (300 mM): (a) compounds **20** (●), **21** (▲) and **28** (■); (b) compounds **12** (Δ), **13** (○) and **29** (□). The insert shows the EPR spectra for the compounds **21** (a) and **13** (b) solutions before illumination (dark) and after 150 min of illumination.

the same EPR hyperfine triplet due to the nitron group in the PBN molecule (^{14}N , $I=1$ and $\sim 100\%$ natural abundance) with a hyperfine splitting a_N of 1.54 ± 0.01 mT and a g -factor of 2.007 ± 0.001 . This hyperfine splitting is characteristic of final PBN-OH \cdot spin adducts, which are expected after self-dismutase of superoxide [30]. Both OH \cdot and O $_2^{\cdot-}$ PBN-adducts have been unambiguously identified by their superhyperfine splitting in ^{17}O -enriched systems, i.e., $a_N = 1.48$ mT for PBN-O $_2^{\cdot-}$ and $a_N = 1.53$ – 1.55 mT for PBN-OH \cdot [31].

The insert in Fig. 4 shows three typical EPR spectra, one in the dark before illumination and two others after 30 and 150 min of UVA laser illumination (375 nm and 16 mW). The error bars in the absolute spin adduct concentration are derived from the uncertainties in the fit parameters of the TEMPOL calibration curve.

Fig. 5(a) and (b) shows the time evolution curves for the concentration of the photogenerated PBN spin adducts for all of the fullerene derivatives synthesized in this work. The same EPR parameters (microwave frequency and power) and concentrations are used for all of the fullerene derivative solutions. While Fig. 5(a) shows the three compounds that have lower efficiency in generating free radicals and thus PBN spin adducts, Fig. 5(b) shows those with higher efficiencies.

According to the well-known photo-oxidation type II mechanism [32], the first step for the production of singlet oxygen ($^1\text{O}_2$) is photoexcitation of the photosensitizers, which are the fullerene compounds in this study. The photoexcited fullerenes enter their higher excited singlet states and are converted by intersystem-crossing into long-lived triplet states. From the triplet state, the available excess energy is transferred to oxygen molecules, thus forming $^1\text{O}_2$. The fullerenes decay to their singlet ground state, where they remain unchanged after this cycle. Although it is well established that the $^1\text{O}_2$ is the main ROS produced by the photoexcitation of fullerenes [32], the formation of superoxide ($\text{O}_2^{\bullet-}$) radicals may occur because of two reasons: (i) photo-oxidation mechanism type I, which is the photo-assisted transfer of an electron from the fullerene to the oxygen molecule during photoexcitation (which may also occur in parallel to the type II mechanism) or (ii) the singlet oxygen reduction process, which is its conversion into superoxide after accepting an electron from another electron donor (such as the photosensitizer molecule). The reduction process of singlet oxygen into superoxide has been previously observed in biological systems [33]. The dismutase of superoxide into highly reactive OH^\bullet [34,35], in the absence of anti-oxidants, is what causes escalating damage in biomolecules, cells and tissues by OH^\bullet , fundamental for PDT.

In a recent paper [20], we have indirectly observed the first stages of this process (conversion of $^1\text{O}_2$ into $\text{O}_2^{\bullet-}$) for a tetrazole-derivative in air-saturated toluene solutions (compound **5** in [20]), which is similar to **3** of this study (differing only in the length of the side-chains). From these experiments we concluded that the main formation of $\text{O}_2^{\bullet-}$ occurred via the type II mechanism followed by the reduction of singlet oxygen into superoxide. The type I mechanism also occurred but to a lesser degree. For that reason, and because $\text{PBN}^{\cdot-}\text{O}_2$ paramagnetic adducts are not known [36], we have performed PBN spin-trapping experiments under UVA illumination in the presence of two distinct ROS inhibitors: superoxide dismutase (for $\text{O}_2^{\bullet-}$) and beta-carotene for ($^1\text{O}_2$).

In this work, we examine in detail the formation of singlet oxygen and superoxide under UVA illumination of toluene solutions containing the new fullerene derivatives and compare the results to pure C_{60} and C_{60} -PCBM solutions. All of the illumination curves (Figs. 4 and 5) formed after the self-dismutase of superoxide (and therefore the evolution of the amount of identified PBN-OH^\bullet adducts), as a function of illumination time, are carefully fitted to a sigmoid function, which is characteristic of irreversible autocatalytic reactions $A + B \rightarrow 2B$ [37]. In our case, the autocatalytic reaction can be viewed as the reduction of the singlet oxygen into superoxide in a closed system, with a further one-to-one conversion of superoxide into OH^\bullet , which is captured by the PBN. The autocatalytic reaction is given by



For this model, a number of assumptions are made: (i) that the type II mechanism is dominant at the beginning of the illumination, producing much more singlet oxygen than superoxide; (ii) the small

amount of superoxide produced at the same time (but to a lesser degree by the type I mechanism) catalyzes the reduction of the singlet oxygen into superoxide; and (iii) the formation of the PBN-OH^\bullet spin adducts after the superoxide self-dismutase into OH^\bullet . For higher concentrations of superoxide, the reduction runs faster. In the end, all of the singlet oxygen is converted into superoxide, and all of the dismutated superoxide generates PBN-OH^\bullet spin adducts. The kinetic equation related to the reduction is

$$\frac{\partial[\text{O}_2^{\bullet-}]}{\partial t} = K[{}^1\text{O}_2][\text{O}_2^{\bullet-}] = K[\text{O}_2^{\bullet-}](N - K[{}^1\text{O}_2][\text{O}_2^{\bullet-}]), \quad (2a)$$

$$[\text{O}_2^{\bullet-}] = [\text{PBN} - \text{OH}^\bullet], \quad (2b)$$

where K is the reaction time constant and N is the total number of produced ROS species that are conserved in a closed system:

$$N = [{}^1\text{O}_2] + [\text{O}_2^{\bullet-}] = [{}^1\text{O}_2]_0 + [\text{O}_2^{\bullet-}]_0 = [\text{PBN} - \text{OH}^\bullet]. \quad (3)$$

The time evolution of the superoxide concentration or the PBN spin adducts is given by the solution of Eq. (2):

$$[\text{O}_2^{\bullet-}] = [\text{PBN} - \text{OH}^\bullet] = \frac{N}{1 + R_0 e^{-KNt}}, \quad (4)$$

where $R_0 = [{}^1\text{O}_2]_0/[\text{O}_2^{\bullet-}]_0$ is the ratio between the amount of singlet oxygen and superoxide produced at the beginning of the reduction. Instead of a single exponential curve, as considered in our previous work [20], the sigmoid functions characteristic of autocatalytic reactions show a better fit for all of the time evolution curves. These are totally consistent with the type I and II reaction mechanisms for the production of superoxide and singlet oxygen, respectively, and they also take into account the efficient reduction of singlet oxygen into superoxide. The fit parameters for the illumination curves for all of the investigated compounds are shown in Table 1.

Notably, the total amounts of ROS produced for all compounds under illumination at saturation, measured in terms of spin adducts/mL, are on the same order, between 0.7 and 3.4×10^{16} (column N, Table 1). These results confirm that the exohedral functionalizations of the fullerenes via cyclopropanation with different organic moieties do not significantly change the photochemical and photophysical properties of the fullerene molecule. This number, however, does not reflect the individual efficiencies in the formation of ROS because we illuminated the solutions with monochromatic light (375 nm) and their molar extinction coefficients differ slightly (Table 1 and Fig. 4). Therefore, the absorbed energy is also different for each sample, and the total amount of spin adducts for each compound must be normalized by the absorbed laser power. If we divide the absolute amount of spin adducts generated at saturation by the absorbed power and the number of fullerene molecules, a merit figure can be calculated that allows for comparison of the overall photosensitizer efficiencies for ROS production for each fullerene compound. We refer to this merit figure as the absolute ROS photogeneration efficiency, which is the absolute amount of ROS produced for each fullerene molecule per

Table 1

Fit parameters for the illumination curves using an autocatalytic sigmoidal curve: the total number of ROS species produced N , the kinetic constant K , the ratio between the amount of singlet oxygen and superoxide produced at the beginning of the reduction R_0 , the monochromatic efficiency and the coefficient of determination of the fit r^2 .

Compound	N (10^{16} spin adducts/mL)	K (10^4 mL/mol s)	R_0	Efficiency at 375 nm (10^{-6} mW $^{-1}$)	r^2
28	1.31(2)	2.7(2)	10.8(7)	0.58(2)	0.995
20	0.70(4)	3.6(7)	3.4(4)	0.17(2)	0.989
21	2.22(7)	1.5(1)	16(2)	1.13(6)	0.996
29	2.78(3)	1.40(6)	8.1(4)	1.32(4)	0.950
13	2.38(9)	1.4(2)	14(2)	1.82(9)	0.992
12	3.34(4)	1.64(9)	13(1)	2.39(6)	0.998
C_{60}	1.84(4)	2.1(1)	9.2(6)	0.92(4)	0.987
C_{60} -PCBM	2.04(6)	2.2(2)	10(1)	0.54(4)	0.996

1 mW of monochromatic illumination at 375 nm. Despite the fact that this merit figure varied roughly within an order of magnitude, as shown in Table 1, we can still draw some conclusions comparing all of the investigated fullerene compounds: (i) pure fullerene is not the most efficient photosensitizer among the molecules investigated; (ii) the more efficient photosensitizers, compared to C₆₀, are compounds 12 and 13. Before further discussing these conclusions, we must also note that the more efficient photosensitizers also have smaller kinetic reaction constants *K*, indicating that they are faster in the production of ROS and therefore saturate more rapidly. In addition, *R*₀, which quantifies how much of the type II mechanism occurs in comparison with type I, is also higher for 12 and 13.

Pure fullerene, with its high efficiency in the production of singlet oxygen, is not the most efficient photosensitizer among those we have investigated. The fact that the [60]fullerene may aggregate in solution diminishes the exposition of the molecules to the dissolved oxygen, thus reducing its efficiency in the formation of ROS. Therefore, functionalization with long moieties likely hinders the aggregation and enhances ROS production. Although compounds 12 and 13 have similar structures, both with a benzyl group bound to the tetrazol unit by an exposed carbon, they exhibit higher ROS photogeneration efficiencies. Apparently, the presence of a benzyl group is important for increasing the production of ROS, which may be due to a higher solubility of these compounds or to the special reactivity of the benzyl group.

For all of the functionalized fullerene compounds, the dominant photophysical process is a type II mechanism in non-polar solvents, leading to the production of singlet oxygen, even though it was recently shown that the type I mechanism is dominant in aqueous solutions [38]. Despite this fact, superoxide radicals (and OH[•]) are also final products even in organic solvents. Here it is important to remember that fullerenes are good electron acceptors in dark conditions; however, under UVA light, they may also donate electrons created by photoionization. The high efficiency for ROS production in these compounds makes them promising photosensitizers for topic PDT and, in particular, for special pharmaceutical formulations in sunscreens or other lotions that do not require high water solubility [39–42].

4. Conclusions

Herein, we presented the synthesis and characterization of six new [6,6]-closed fullerene cycloadducts bearing five-membered heterocyclic wings by a simple and efficient synthesis route. All of the compounds synthesized in this work have been investigated as potential photosensitizers for PDT using an EPR spin-trapping methodology and compared with pure C₆₀ and C₆₀-PCBM. Their optical absorption spectra are very similar, showing strong absorption bands in the near UVA spectral region. On average, all of the compounds produce between 0.2 and 2.4 ROS per 10⁶ molecules and per mW of laser power at 375 nm (compared to 1 ROS for C₆₀). The exohedral functionalization of fullerenes with heterocyclic wings does not drastically alter the photochemical and photophysical properties of the fullerenes. However, compared to C₆₀, the most efficient compounds, **12** and **13**, may owe their enhanced efficiency to the additional degree of liberty introduced by the methylenic carbon of the benzyl group, through either less aggregation and/or by a special reactivity of the benzyl. Additionally, we can speculate that the presence of a benzylic carbon, which is highly reactive in radical reactions, may play an important role in enhancing this efficiency [43].

For all of the fullerene compounds, the photo-oxidation process in the non-polar solvent toluene can be explained by an autocatalytic reaction mechanism involving type I and type II mechanisms,

with the latter being dominant in the initial stage of illumination. In the saturation stage, all ROS produced are converted into OH[•] via the self-dismutase of superoxides. These results show that the hydrophobic fullerene compounds are potential photosensitizers for topical PDT.

Acknowledgements

The authors are grateful to the Brazilian research foundations CAPES, CNPq, FAPEMIG, FAPESP and the Instituto de Nanotecnologia (MCT) for research grants and financial support.

Appendix A. Supplementary data

Supplementary data associated with this article can be found, in the online version, at doi:10.1016/j.jphotochem.2010.10.007.

References

- [1] H.W. Kroto, J.R. Heath, S.C. O'Brien, R.F. Curl, R.E. Smalley, C₆₀: Buckminsterfullerene, *Nature* 318 (1985) 162–163.
- [2] W. Krätschmer, L.D. Lamb, K. Fostiropoulos, D.R. Huffman, Solid C₆₀: a new form of carbon, *Nature* 347 (1990) 354–358.
- [3] P. Innocenzi, G. Brusatin, M. Guglielmi, R. Signorini, M. Meneghetti, R. Bozio, M. Maggini, G. Scorrano, M. Prato, Optical limiting devices based on C₆₀ derivatives in sol–gel hybrid organic–inorganic materials, *J. Sol–Gel Sci. Technol.* 19 (Special issue) (2000) 263–266.
- [4] D. Felder, D. Guillon, R. Lévy, A. Mathis, J.F. Nicoud, J.F. Nierengarten, J.L. Rehspringer, J. Schell, A water soluble methanofullerene derivative: synthesis, micellar aggregation in aqueous solutions, and incorporation in sol–gel glasses for optical limiting applications, *J. Mater. Chem.* 10 (2000) 887–892.
- [5] Y. Mikata, S. Takagi, M. Tanahashi, S. Ishii, M. Obata, Y. Miyamoto, K. Wakita, T. Nishisaka, T. Hirano, T. Ito, M. Hoshino, C. Ohtsuki, M. Tanihara, S. Yano, Detection of 1270 nm emission from singlet oxygen and photocytotoxic property of sugar-pendant [60]fullerenes, *Bioorg. Med. Chem. Lett.* 13 (2003) 3289–3292.
- [6] T. Da Ros, G. Spalluto, A.S. Boutorine, R.V. Bensasson, M. Prato, DNA-photocleavage, *Curr. Pharm. Des.* 7 (2001) 1781–1821.
- [7] P. Mroz, G.P. Tegos, H. Gali, T. Wharton, T. Sarna, M.R. Hamblin, Photodynamic therapy with fullerenes, *Photochem. Photobiol. Sci.* 6 (2007) 1139–1149.
- [8] Y. Tabata, Y. Ikada, Biological functions of fullerene, *Pure Appl. Chem.* 71 (1999) 2047–2053.
- [9] H. Hoppe, N.S. Sariciftci, Organic solar cells: an overview, *J. Mater. Res.* 19 (2004) 1924–1945.
- [10] M.S. Bjelaković, D.M. Godjevac, D.R. Milić, Synthesis and antioxidant properties of fullerene-steroidal covalent conjugates, *Carbon* 45 (2007) 2260–2265.
- [11] S. Bosi, T. Da Ros, G. Spalluto, M. Prato, Fullerene derivatives: an attractive tool for biological applications, *Eur. J. Med. Chem.* 38 (2003) 913–923.
- [12] T. Da Ros, M. Prato, Medicinal chemistry with fullerenes and fullerene derivatives, *Chem. Commun.* 8 (1999) 663–669.
- [13] M. Satoh, I. Takayanagi, Pharmacological studies on fullerene (C₆₀), a novel carbon allotrope, and its derivatives, *J. Pharmacol. Sci.* 100 (2006) 513–518.
- [14] J.F. Nierengarten, Chemical modification of C₆₀ for materials science applications, *New J. Chem.* 28 (2004) 1177–1191.
- [15] J.F. Nierengarten, M.G. Nava, S. Zhang, P. Masson, L. Oswald, C. Bourgoigne, Y. Rio, G. Armario, S. Setavesh, Fullerene-containing macromolecules for materials science applications, *Carbon* 42 (2004) 1077–1083.
- [16] A. Ray, K. Santhosh, S. Chattopadhyay, A. Samanta, S. Bhattacharya, Spectroscopic and theoretical investigations on effective and selective interaction of fullerenes C₆₀ and C₇₀ with a derivatized Zn–phthalocyanine: stabilization of charge-recombined state by side-on approach of C₇₀, *J. Phys. Chem. A* 114 (2010) 5544–5550.
- [17] L.O. Husebo, B. Sitharaman, K. Furukawa, T. Kato, L.J. Wilson, Fullerenols revisited as stable radical anions, *J. Am. Chem. Soc.* 126 (2004) 12055–12064; G.C. Alves, L.O. Ladeira, A. Righi, K. Krambrock, H.D. Calado, R. Gil, M.V.B. Pinheiro, Synthesis of C₆₀(OH)_{18–20} in aqueous alkaline solution under O₂-atmosphere, *J. Brazil. Chem. Soc.* 17 (2006) 1186–1190.
- [18] J. Iehl, R.P. Freitas, B.D. Nicot, J.F. Nierengarten, Click chemistry for the efficient preparation of functionalized [60]fullerene hexakis-adducts, *Chem. Commun.* 21 (2008) 2450–2452.
- [19] X. Chen, C.Y. Liu, T.H. Jen, S.A. Chen, S. Holdcroft, Synthesis and characterization of a fullerene bearing a triazole group, *Chem. Mater.* 19 (2007) 5194–5199.
- [20] L.J. Santos, R.B. Alves, R.P. Freitas, J.F. Nierengarten, L.E.F. Magalhães, K. Krambrock, M.V.B. Pinheiro, Production of reactive oxygen species induced by a new [60]fullerene derivative bearing a tetrazole unit and its possible biological applications, *J. Photochem. Photobiol. A: Chem.* 200 (2008) 277–281.
- [21] F.C. Da Silva, V.F. Ferreira, M.C.B.V. De Souza, Adaptação de forno de microondas doméstico para realização de reações de transesterificação sob refluxo e catálise por argilas, *Quim. Nova* 29 (2006) 376–380.
- [22] G.L. Kad, I. Kaur, M. Bhandari, J. Singh, J. Kaur, Functional group transformations of diols, cyclic ethers, and lactones using aqueous hydrobromic acid and phase

- transfer catalyst under microwave irradiation, *Org. Process Res. Dev.* 7 (2003) 339–340.
- [23] D.C. Johnson, T.S. Widlanski, Cerium(III) chloride-mediated reactions of sulfonamide dianions, *J. Org. Chem.* 68 (2003) 5300–5309.
- [24] A.H. Klier, R.J. Alves, M.A.F. Prado, J.D.S. Filho, N.B. D'Accorso, Synthesis of new five membered nitrogen containing heterocycles bearing D-galactose side chains, *Synth. Commun.* 30 (2000) 4361–4374.
- [25] A.F. Brigas, Product class 30: tetrazoles, *Sci. Synth.* 13 (2004) 861–915.
- [26] L.J. Santos, I. Luduvico, M.R. Couri, R.B. Alves, M.A.F. Prado, R.P.F. Gil, Synthesis of new tetrazole derivatives of α,α -trehalose, *Synth. Commun.* 37 (2007) 3059–3066.
- [27] C. Bingel, Cyclopropanierung von fullerenen, *Chem. Berl.* 126 (1993) 1957–1959.
- [28] J.F. Nierengarten, T. Habicher, R. Kessinger, F. Cardullo, F. Diederich, Macrocyclization on the fullerene core: direct regio- and diastereoselective multi-functionalization of [60]fullerene, and synthesis of fullerene-dendrimer derivatives, *Helv. Chim. Acta* 80 (1997) 2238–2276.
- [29] F. Diederich, L. Isaacs, D. Philp, Syntheses, structures, and properties of methanofullerenes, *Chem. Soc. Rev.* 23 (1994) 243–255.
- [30] E. Finkelstein, G.M. Rosen, E.J. Rauckman, Spin-trapping kinetics of the reaction of superoxide and hydroxyl radicals with nitrones, *J. Am. Chem. Soc.* 102 (1980) 4994–4999.
- [31] C. Mottley, H.D. Connor, R.P. Mason, [^{17}O]oxygen hyperfine structure for hydroxyl and superoxide adducts of the spin traps DMPO, PBN and 4-POBN, *Biochem. Biophys. Res. Commun.* 141 (1986) 622–628.
- [32] J.W. Arbogast, A.P. Darmanyan, C.S. Foote, Y. Rubin, F.N. Diederich, M.M. Alvarez, M. Alvarez, S.J. Anz, Photophysical properties of sixty atom carbon molecule (C_{60}), *J. Phys. Chem.* 95 (1991) 11–12.
- [33] G. Peters, M.A.J. Rodgers, On the feasibility of electron transfer to singlet oxygen from mitochondrial components, *Biochem. Biophys. Res. Commun.* 96 (1980) 770–776.
- [34] G.M. Rosen, B.E. Britigan, H.J. Halpern, S. Pou, *Free Radicals: Biology and Detection by Spin Trapping*, Oxford University Press, Oxford/New York, 1999.
- [35] E. Finkelstein, G.M. Rosen, E.J. Rauckman, J. Paxton, Spin-trapping superoxide, *Mol. Pharmacol.* 16 (1979) 676–685.
- [36] J.R. Harbour, S.L. Issler, M.L. Hair, Singlet oxygen and spin trapping with nitrones, *J. Am. Chem. Soc.* 102 (1980) 7778–7779.
- [37] E. Arslan, I.J. Laurenzi, Kinetics of autocatalysis in small systems, *J. Chem. Phys.* 128 (2008) 015101.
- [38] Y. Yamakoshi, N. Umezawa, A. Ryu, K. Arakane, N. Miyata, Y. Goda, T. Masumizu, T. Nagano, Active oxygen species generated from photoexcited fullerene (C_{60}) as potential medicines: $\text{O}_2^{\bullet-}$ versus $^1\text{O}_2$, *J. Am. Chem. Soc.* 125 (2003) 12803–12809.
- [39] Y. Nakajima, T. Yagami, K. Fukuhara, S. Sueyoshi, N. Miyata, Solubilization of fullerenes into water with polyvinylpyrrolidone applicable to biological tests, *J. Chem. Soc. Chem. Commun.* 4 (1994) 517–518.
- [40] L. Wenzhu, Q. Kaixian, H. Wendong, Z. Xinxin, C. Wanxi, Water soluble C_{60} -liposome and the biological effect of C_{60} to human cervix cancer cells, *Chin. Phys. Lett.* 11 (1994) 207–210.
- [41] J. Liu, S.I. Ohta, A. Sonoda, M. Yamada, M. Yamamoto, N. Nitta, K. Murata, Y. Tabata, Preparation of PEG-conjugated fullerene containing Gd^{3+} ions for photodynamic therapy, *J. Control. Release* 117 (2007) 104–110.
- [42] A. Ikeda, T. Sue, M. Akiyama, K. Fujioka, T. Shigematsu, Y. Doi, J.-I. Kikuchi, T. Konishi, R. Nakajima, Preparation of highly photosensitizing liposomes with fullerene-doped lipid bilayer using dispersion-controllable molecular exchange reactions, *Org. Lett.* 10 (2008) 4077–4080.
- [43] C.J. Mattia, C.P. Lebel, S.C. Bondy, Effects of toluene and its metabolites on cerebral reactive oxygen species generation, *Biochem. Pharmacol.* 42 (1991) 879–882.